Astron. Astrophys. 328, 371–380 (1997)

ASTRONOMY AND ASTROPHYSICS

Chromospheric evidence for magnetic reconnection

A. Falchi[1], **J. Qiu**[1⋆], **and G. Cauzzi**[2]

[1] Osservatorio Astrofisico di Arcetri, Largo E. Fermi 5, I-50125 Firenze, Italy
[2] Osservatorio Astronomico di Capodimonte, via Moiariello 16, I-80131 Napoli, Italy

Received 18 March 1997 / Accepted 5 August 1997

Abstract. We study the decay phase of an M2.6 flare, observed with ground based instruments at NSO/Sac Peak and with the cluster of instruments onboard *Yohkoh*. The whole set of chromospheric and coronal data gives a picture consistent with the classical Kopp-Pneuman model of two-ribbon flares. We clearly witness new episodes of coronal energy release, most probably due to magnetic reconnection, during the decaying phase of the flare. Within the newly created chromospheric ribbons, we identify several small kernels, footpoints of magnetic loops involved in the flare, where energy is probably deposited by a conduction front from coronal sources. The presence of a source (T_e=22 MK, and EM=5.$\times 10^{48}$ cm^{-3}) thermally emitting in the 14-23 keV energy band confirms this hypothesis.

A new, interesting observational result is given by the measure of chromospheric downflows in different parts of the flaring kernels. For all the cases examined, we find a stronger downflow at the outer edge of the flaring structure. The flows have amplitude of tens of km s^{-1}, over regions only a few arcsec across, and seem to decrease when the flaring kernels slow their motion on the solar surface and fade away. We believe that these downflows directly map the outer boundary magnetic field lines of the reconnecting loops, as predicted in recent reconnection models that take into account explicity the effects of heat conduction. The flows represent the chromospheric counterpart of coronal features observed in soft X-ray such as cusp-like structures and the temperature stratification in flaring loop systems. The observed amplitude of these chromospheric flows could be an important constraint for quantitative modelling of coronal reconnection mechanisms and their effects on the lower solar atmosphere.

Key words: Sun: activity – chromosphere – corona – flares

1. Introduction

Eruptive flares, a term that encompasses several classifications used in the past ("two-ribbon", "long-decay" or "dynamic" flares), are one of the most interesting activity phenomena on the Sun. While their morphological manifestations vary over a wide range, from eruptions of quiescent filaments (disparition brusque) with no visible flare in H_α, to powerful two-ribbon flares, common characteristics are given by a global magnetic field disruption and processes of energy release long lasting after the end of the impulsive phase. The magnetic reconnection model invoked to interpret these flares postulates that the magnetic field lines, open by some eruptive phenomenon, reconnect to a lower energy state. This reconnection process is very fast in the beginning of the flare and slows down in later phases (Kopp and Pneuman, 1976). The separation of the flare-ribbons at chromospheric level, and the rising of the system of loops in the corona, are considered signatures of the magnetic reconnection processes. During the last few years, the high-resolution images obtained from the Hard X-ray Telescope (HXT) and Soft X-ray Telescope (SXT) on *Yohkoh* have shown features consistent with the hypothesis of a reconnection site in the corona. In particular, a hard X-ray source located above the soft X-ray loops (Sakao et al., 1992; Masuda et al., 1994) and the cusp-like loop structure, suggestive of a reconnection site (Tsuneta et al. 1992; Tsuneta, 1996), support the idea that magnetic reconnection occurs above the loop top. Aschwanden et al. (1996) measured the electron time-of-flight distances for 5 flares presenting a Hard X-ray (HXR) double footpoint source in addition to a HXR source in the loop cusp, and found that the heights of the HXR source are consistent with the electron time-of-flight distance to the footpoints. This provides further evidence to the idea that particle acceleration occurs in the cusp region above the flare loop.

During the impulsive phase, when the reconnection rate rapidly increases, the loop top shows a high temperature region (Tsuneta, 1996), and it is plausible to assume that the chromosphere might be heated by non thermal-electron impact (thick target model) and/or by thermal conduction from this region. The response of the chromosphere to both energy deposition mechanisms is a strong chromospheric evaporation together with a chromospheric condensation moving downward (Fisher, 1989; Gan et al., 1991). The blue-shifted emission component of X-ray spectral lines observed in several flares (Antonucci et al., 1982) is considered a signature of the chromospheric evapora-

⋆ Astronomy Dept., Nanjing University, China

tion and the red-shifted emission of chromospheric lines (Ichimoto & Kurokawa, 1984; Canfield et al., 1990; Falchi et al., 1992) a signature of the condensation motion.

In the case of a two ribbon flare, it is generally assumed that the outer edges of the chromospheric ribbons are the footpoints of newly reconnected hot coronal loops, whereas the inner edges are the roots of cooling loops that later might become visible in H_α (Moore et al. 1980, Švestka 1989). In a partial revision of earlier reconnection models, Forbes & Acton (1996) found that, if the magnetic fields are sufficiently strong, the reconnecting magnetic field lines map in the chromosphere only to a thin region ($\approx 1''$) of downward moving chromospheric plasma at the outer edge of the ribbons. Hence, the line-of-sight velocity in different regions of the chromospheric ribbons during an eruptive flare may be a powerful diagnostic of the processes taking place at coronal levels, in particular of magnetic reconnection. An earlier report of peculiar effects on the outer border of a two-ribbon flare was given by Švestka et al. (1980), that discussed a set of multi-slit observations. They briefly reported of small and very short-lived red-shifts in the H_α line profiles along the outer edges of the ribbons in an eruptive flare, but did not specify the spatial dimensions of the red-shifts, nor their amplitude. To our knowledge, other systematic spectral observations of two-ribbon flares are available in the literature only for the late phase, when post-flare loops are already formed (Schmieder et al., 1987; Gu et al., 1992).

We report in this paper about flare observations obtained during a coordinated campaign between *Yohkoh* and ground based instruments, mainly the facilities of National Solar Observatory (both Kitt Peak and Sac Peak sites). In particular, we will describe an eruptive, two-ribbon flare (GOES class M2.6), observed on February 4, 1995. Qiu et al. (1997, Paper I) studied the pre-flare and impulsive phase of this event, characterized by a filament eruption and the subsequent formation of two bright ribbons at chromospheric level. In this paper we study the decay-phase after the maximum emission both in H_α and soft X-ray (SXR). We will concentrate on the study of new chromospheric ribbons, formed simultaneously with new episodes of energy release at coronal level, in order to look for evidence of chromospheric signatures of the reconnection processes. The data are briefly illustrated in Sect. 2, as well as some of the flare characteristics. The flare evolution is described in Sect. 3 both at chromospheric and at coronal levels, while a possible scenario is discussed in Sect. 4. The motions observed in the ribbons are reported and discussed in Sect. 5, and conclusions are given in Sect. 6.

2. Observational data

On February 4, 1995, an eruptive flare (GOES class M2.6) developed in active region NOAA 7834 (μ=0.95), in the time interval 15:42-16:39 UT. The maximum H_α emission occurred at 15:43 UT (Solar Geophysical data).

At the onset of the eruptive flare, *Yohkoh* was just coming out of its night, so the impulsive phase was observed only with the Wide Band Spectrometer (WBS, Yoshimori et al., 1991) in the energy channels from 20 to 91 keV. Later on during the flare development, the signal was too low to be recorded with this instrument. The Soft X-ray Telescope (SXT, Tsuneta et al., 1991) and the Hard X-ray telescope (HXT, Kosugi et al., 1991) began the observations in flare mode around 15:46 UT, for an interval of about 10 minutes. SXT obtained images (FOV = $157'' \times 157''$, $2.46''$/pxl) with the aluminum (Al12) and beryllium (Be119) filters, with a time resolution ranging between 2 and 6 s. The HXT recorded data in Pulse Height Mode (PHM) with 8 s time resolution; we could obtain images only in the lowest energy Lo channel (14-23 keV), due to the low emission in higher energy bands. The HXT images (FOV = $158'' \times 158''$, pointing resolution $\sim 5''$) were recovered with an integration time of about 50 s and coaligned with SXT images (Masuda, 1994). The coalignment of *Yohkoh* images with our photospheric and chromospheric observations was obtained using the full disk observations of the Mees White Light Telescope (Wülser, 1996). The Bragg Crystal Spectrometer (BCS, Culhane et al., 1991) recorded spectra in the three channels S XV, Ca XIX and Fe XXV, without spatial resolution, from 15:46 UT up to 15:53 UT. In the following analysis, we will mainly use the Fe XXV data.

For the general description of the available ground based observations we refer to Paper I. We recall that images of the flare region, with filters in different bands, were acquired with the Vacuum Tower Telescope (VTT) at NSO/SP from 15:31 to 16:08 UT, with a typical temporal resolution of few seconds and a spatial resolution of about $1''$. Spectra in the range 3750-4150 Å were acquired with the Universal Spectrograph (USG) from 15:43:00 until 15:56:03 UT, with the slit moving on different positions in the FOV. This spectral range contains both the CaII K and H_δ lines, that we use to provide a diagnostic of plasma flows in the chromosphere. Finally, full disk magnetic maps were available from NSO/Kitt Peak after 18:00 UT.

3. Flare evolution

3.1. Overview

The temporal evolution of the global emission is given in the light-curves of Fig. 1.

The impulsive phase is characterized by a sharply peaked HXR emission, measured with the WBS in energy bands up to 81-91 keV, and lasts about 90 s (Fig. 1-a). During this phase, at chromospheric levels two bright ribbons develop very rapidly; the ribbons are shown as R1 and R2 in Fig. 2-a, at the time of maximum emission. Their peculiar shape follows the magnetic inversion line, displayed in Fig. 2-a with the solid contour, which surrounds an island of negative polarity just south of the main (positive) spot. For a more detailed description of the magnetic field of the region we refer to Paper I.

As said previously, several *Yohkoh* instruments started observing at 15:46 UT, when the flare was already in the decaying phase. In Fig. 1-b we show the light curves of the total flux in the BCS resonance lines (Fe XXV and S XV), of the total flux in the SXT Be filter images, and the hard-X ray light curve obtained in the HXT 14-23 keV Lo-channel. The BCS S XV and

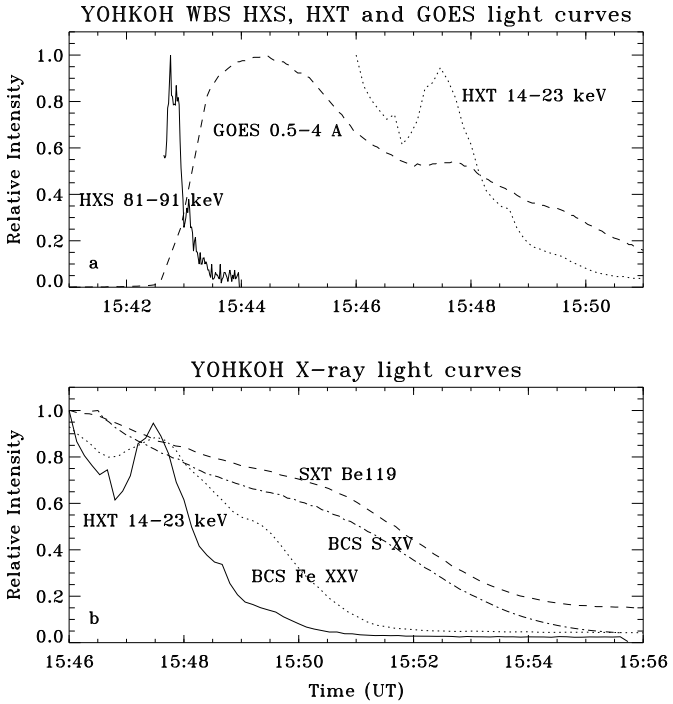

Fig. 1. a X-ray light curves, given in arbitrary units and normalized to the peak value, during the whole flare development. **b** X-ray light curves, for the second phase of the flare, for several instruments aboard *Yohkoh*

SXT Be119 light curves have a smooth shape with a decreasing time of about 5 minutes, while the Fe XXV and the HXT light curves have a shorter decreasing time of about 1.5 minutes and show a maximum at about 15:47:30 UT. Since the wavelength of the S XV channel and the center of the Be119 filter transmission are both at ∼5 Å, it is understandable that the two light curves have the same shape (Feldman et al., 1994). The Fe XXV channel and the sensitivity curve of the filter Lo-HXT are not centered at the same energy. However, the line emissivity function peaks at a very high electron temperature of about 50 MK (much more than the temperature of Ca XIX and S XV); the BCS - Fe XXV channel hence is sensitive to the emission of hot plasma that might be responsible also for the emission measured by the HXT (Fludra et al., 1995).

At chromospheric level, the flare decaying phase is characterized by the weakening of the ribbons R1 and R2, and by the development of new bright features along another portion of the magnetic neutral line, closer to the spot (Fig. 2-b). This suggests that another portion of the coronal arcade of magnetic loops, connecting the negative polarity island with its magnetically positive surroundings, becomes involved in the instability processes causing the flare. The new flaring structures are an extension of the old ribbons (although their general enhancement never reaches the level of R1 and R2), and they also spread apart from the magnetic neutral line. Within these new ribbons we can identify several smaller kernels, of a few arcsec size, that brighten at different times in different locations, without following a clear sequence. These kernels and their properties will be described in detail in the next sections.

Both the secondary maximum measured in different X-ray energy bands, and the new bright chromospheric kernels, support the idea of new episodes of coronal energy release, taking place during the decaying phase of this flare.

3.2. Chromospheric and coronal structures

Due to the saturation of some of the H_α line center images, we describe the chromospheric evolution of the flare at other wavelengths, especially H_α + 1.5 Å, for which we have a temporal resolution of 2.5 s. In Fig. 3 we show H_α + 1.5 Å images at different times, starting from 15:45:30.

We see that some small features, already present in the positive polarity ribbon R1 during the impulsive phase (B1 and C1 in Fig 3-a), are now reinforced, and new bright structures (A1 and A2) become visible. A1 and A2 are small regions, 4-6″ in size, and extend, respectively, the ribbons R1 and R2. They are located on opposite sides of the magnetic neutral line and reach their maximum emission contemporaneously, at 15:45:45 UT (Fig. 4-a). At 15:47:30 UT the patch A1 is not visible anymore, while A2 reaches a new maximum (Fig. 3-c and 4-a) and becomes visible also in the He D3 line. This is simultaneous with a maximum, in both H_α + 1.5 Å and He D3, of kernel B1, that in the meantime has moved about 3-4″ towards the spot (Fig. 3-c and 4-b). The continuum light curves of all the kernels remain constant throughout this phase, while during the impulsive phase at least one flaring kernel showed an increase of ∼ 6% of the continuum emission (see Paper I).

Images from SXT and HXT begin at this time, and their contours are overlayed on the H_α + 1.5 Å images starting from Fig. 3-b. The SXR emission extends over the bright chromospheric area, with the maximum emitting region located between the patches tracing the new ribbons and a more diffuse emission related to the old weakening ribbons. Due to the acquisition data mode (PHM) and to the low level of emission we could construct only one HXT image, at 15:47:30 UT, with an integration time of about 50 s. The HXR emitting structure is a point-like source (FWHM ∼ 5″, the resolution of the image) that spatially coincides with the chromospheric region A2, while it only partially overlaps with the most intensely emitting SXR region (Fig. 3-c). Later on, at 15:48:45 UT, we don't measure any hard X-ray emission (Fig. 3-d and 4-b), and the emission at all the other wavelengths examined has decreased both in area and intensity (Fig. 3-d).

The X-ray emission maximum in the light curve of the total flux of Fe XXV (1.85 Å), and in the 14-23 keV Lo-channel related to the HXT source, coincide within 5 s to the chromospheric maximum (Fig 4-b).

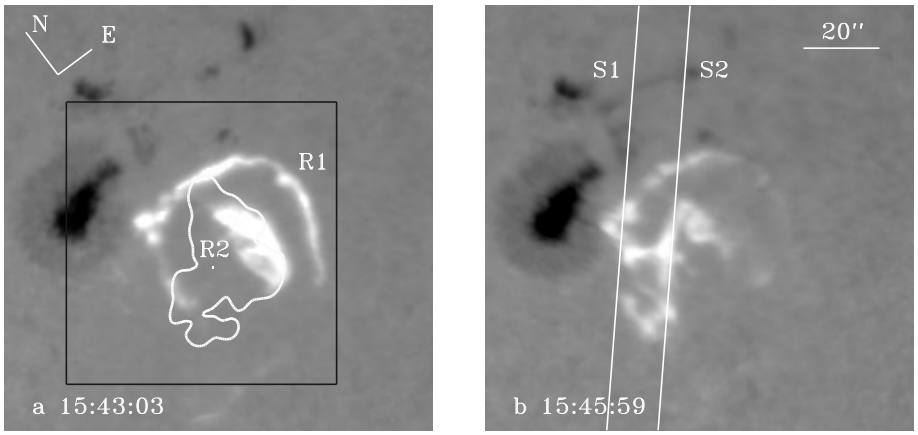

Fig. 2. a H_α + 1.5 Å image of the flaring region at the time of maximum emission. Image scale and orientation are indicated. R1 and R2 are the ribbons that develop during the impulsive phase. The solid contour represents the magnetic neutral line, encircling a negative polarity island within the leading positive polarity. The black square frames the field of view of Fig. 3; **b** Flaring region at a later stage. S1 and S2 are the positions occupied by the USG slit at different times

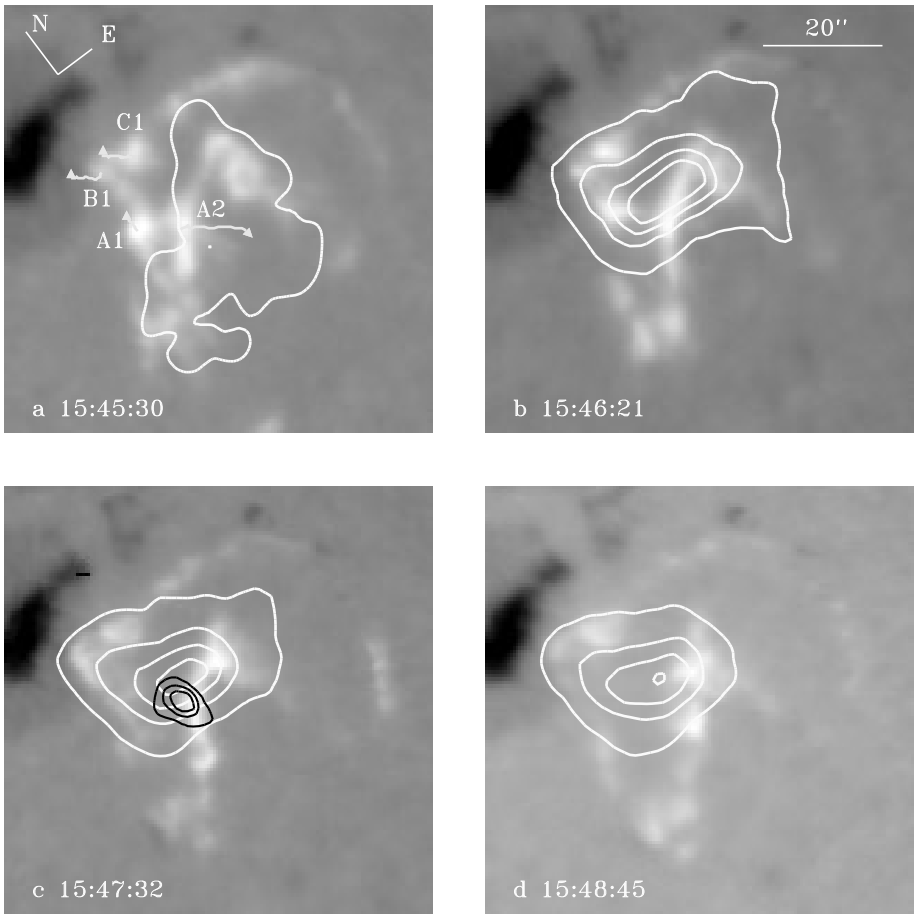

Fig. 3a and b. H_α + 1.5 Å images showing the global evolution of the flare for the smaller field of view framed in Fig. 2. **a** The white contour represents the magnetic neutral line, while letters indicate flaring kernels relevant to the discussion. The solid short lines trace the horizontal motion of these kernels; the arrows give the direction of the motion; **b** SXT emission overlayed on H_α + 1.5 Å image. Contours are at 10, 30, 50, 70% of the global maximum emission. The SXT loops cover both the old and new chromospheric ribbons; **c** Composite image at the time of the secondary HXR maximum. SXT countours are drawn for the same levels of panel **b**, and show that the maximum emission is shifting towards the new ribbons. Black contours define the point-like HXT source. Levels are 20, 40, 60% of maximum emission; **d** Later stage of the flare. The SXT contours now trace essentially the system of loops between the new ribbons

4. Reconnecting loops and a thermal source

What kind of scenario can explain the observations reported in the previous section? Kurokawa et al. (1988) observed different bright kernels, seen in the H_α blue wing on the opposite polarity regions of a two-ribbon flare, that attained their maximum intensity simultaneously within 1 s. This brightening was also simultaneous, within the same temporal resolution, to the maximum of the HXR curve. They argued that the chromospheric kernels are the footpoints of a flaring loop system, heated by non thermal electrons with a time delay of no more than 1 s between them. A similar explanation can be invoked in our case. The temporal coincidence in the maximum emission (15:45:45 UT) of A1 and A2 supports the hypothesis that they are the footpoints of a flaring loop system, heated with a time delay of max. 2.5 s (our time resolution). Even if we have SXT images only at 15:46:20 UT, the presence of a loop system connecting A1 and A2 is evident in Fig. 3-c. We cannot yet draw conclusions about the energy transport mechanism from coronal to chromospheric levels, since we lack HXR light curves at the maximum time.

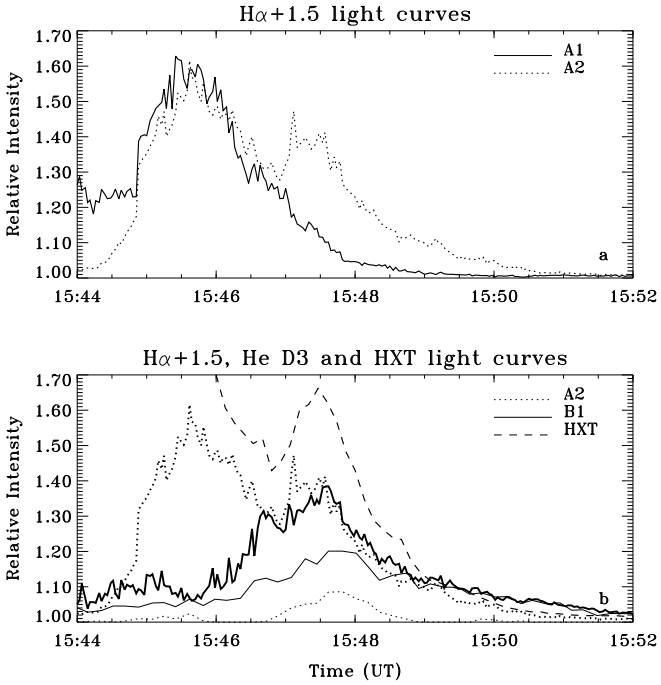

Fig. 4. a H_α + 1.5 Å light curves in the two flaring kernels A1 and A2, belonging to the ribbons R1 and R2 respectively. The curves are normalized to the pre-flare intensity; **b** H_α + 1.5 Å (thick line) and He D3 (thin line) light curves for kernels A2 (dotted) and B1 (solid), together with the global HXR curve in the band 14-23 keV (dashed)

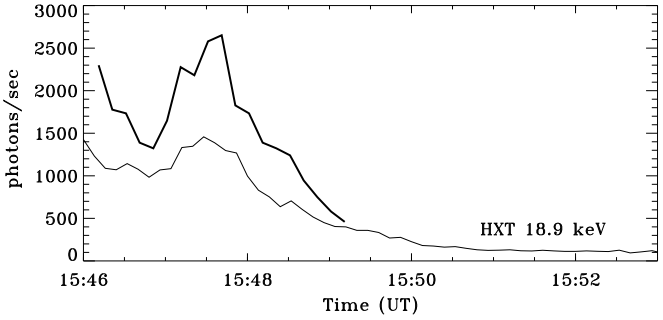

Fig. 5. (Thin line) Photon flux measured in the 18.9 keV band of the Lo-HXT channel. (Thick line) Photon flux computed at 20 keV using the T_e and EM values derived from the spectral analysis of the BCS Fe XXV channel

Evidence suggests that B1 and A2 are the chromospheric footpoints of another loop undergoing a new heating process, as proved by the new brightenings in the H_α wings and in He D3 (Zirin, 1988; Cauzzi et al., 1995). The temporal coincidence between the maximum emission of A2 and B1 at chromospheric level and the maximum emission of the coronal plasma in different energy bands, from 6.7 keV (Fe XXV) up to 23 keV, implies that the heating involves the loop at coronal levels as well. The apparent spatial coincidence of the chromospheric region A2 and the Lo-HXT source (Fig. 3-c), suggests that the HXR emission is mainly located in one of the loop footpoints, i.e. that it is due to non-thermal electrons impacting on the chromosphere (thick-target model, see Brown, 1971; Hudson, 1972; Emslie, 1978, 1983; Sakao, 1994 and references therein).

On the other hand, the similarity of the X-ray light curves (Fe XXV and Lo-HXT, see Sect. 3.1) may be due to the fact that we are watching the emission of the same plasma, i.e. that the plasma emitting in the Fe XXV line could be the same that thermally emits at 14-23 keV. To check this possibility, we can estimate what would be the photons flux in the center of the Lo-HXT channel, produced by the plasma emitting in the Fe XXV line. The temperature T_e and the emission measure EM of such a plasma (T_e=22 MK, EM=5.$\times 10^{48}$ cm^{-3} at the maximum time) were estimated from the spectral analysis using a program in the standard *Yohkoh* software package.

Following Mewe et al. (1986), we compute the photon number emissivity of the considered volume, at photon energy E per unit energy interval (phot s^{-1} keV^{-1})

$$\mathscr{E}(\mathrm{E}, \mathrm{T_e}) = 1.032 \times 10^{-14} \mathrm{G_{ff}} \mathrm{E}^{-1} \mathrm{T_e}^{-0.5} \mathrm{EM} * \exp - \frac{11.6 * \mathrm{E}}{\mathrm{T_e}}$$

using the appropriate Gaunt factor G_{ff} = 1.18 and the center of the Lo-HXT energy band (20 keV) as the photon energy E (Kosugi, 1993). Taking into account the area of the collimators and the efficiency of the detector we obtain a photon flux of the same order of magnitude as the one measured with Lo-HXT and with the same temporal behaviour. In Fig. 5 we show the computed and the measured photon flux; the good agreement between the two curves confirms that the hot plasma detected in the BCS Fe XXV channel emits a sufficient number of high energy photons to be detected with Lo-HXT.

The thermal origin of the HXR emission implies that the emitting plasma is located in the uppermost portion of the magnetic loop. This plasma is probably heated by a reconnection process that locally converts free magnetic energy into thermal and kinetic energy. Part of this thermal energy is transported down to the chromosphere by a conduction front and heats the chromospheric footpoints A2 and B1. We can then argue that the apparent spatial coincidence between A2 and the HXT source is only due to projection effects. If we consider the spatial resolution of HXT ($\sim 5''$), the position of the loop on the solar disk, and its small size ($10''$ radius), we find that the projected location of a coronal loop-top HXT source could well coincide with A2.

We cannot say with certainty which heating mechanism is responsible for the brightening of the kernel pair A1-A2 (and of kernel C1), since we lack direct coronal data. However, if the pair B1-A2, for which we see both H_α and He D3 emission, is heated by conduction, it seems plausible that also the other kernels, for which we don't see any He D3 emission at all, are heated by conduction as well.

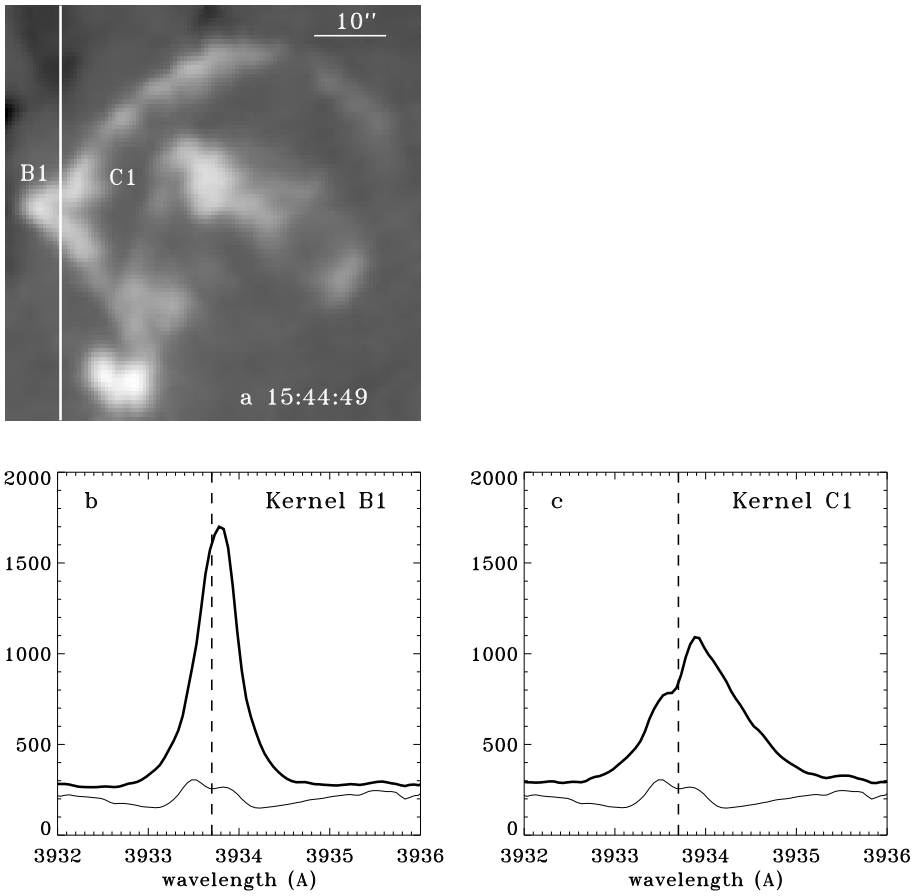

Fig. 6. a H_α + 1.5 Å image of the flaring ribbons showing how slit S1 intersects the bright kernels. The image has been slightly rotated with respect to Figs. 2 and 3. The slit crosses C1 in its outer edge, and B1 in its inner edge; **b**, **c** CaII K profiles in a quiet region (thin line) and in kernels B1 and C1 (thick line). The dashed line is the rest wavelength of CaII K

5. Ribbon motions

5.1. Vertical motion (line-of-sight velocity)

We acquired spectra with the slit of the USG positioned successively in S1 and S2 as indicated in Fig. 2-b. The slits intersect regions of the ribbons R1 and R2 formed during the impulsive phase, and are tangent to sections of the ribbons newly formed during the decay phase. With the slit of the USG in the position S1, we acquired spectra from 15:44:48 until 15:46:52 UT, with a time resolution ranging between 5 and 30 s. We show in Fig. 6-a an enlargement of the ribbon R1 intersected by the slit in this interval: at 15:44:49 the slit is tangent to the inner edge of the structure B1 and crosses the outer edge of the structure C1. We recall that both B1 and C1 developed during the impulsive phase, and had a new brightening around this time. Examples of the corresponding spectra are shown in Fig. 6-b and 6-c respectively. On the inner edge of B1, both the Ca II K line and the H_δ line (not shown in the figure) are in emission, symmetric, with a small red-shift of the line center (Fig. 6-b), while on the outer edge of C1 both lines show a strong red asymmetry in the wings (Fig. 6-c). This asymmetry is stronger for the outermost points of the structure.

At the time of the next spectrum (15:45:22 UT, see Fig. 7-a), the kernel A1 is well developed, almost at its maximum emission, and the USG slit is tangent to its outer edge. No spectral asymmetry was detected in these positions before A1 brightened, but at this later time both the Ca II K line and the H_δ line are in emission and show a red shift of the maximum emission (Fig. 7-b). Along the inner edge of B1 still no asymmetry is detectable, whereas in the points on the outer edge of C1 the red asymmetry is still present (Fig. 7-c,d). Interpreting the red shift as Doppler velocity (for the method used see Cauzzi et al., 1996), we obtain downward velocities on the outer edges of A1 and C1 that are between 10 and 30 ($\pm$ 2) km s^{-1}, and almost no velocity in the points of the inner edge of B1. This is clearly summarized in Fig. 8-a and 8-b, where we show the velocity measured along the slit, at the times reported above, together with the intensity in the center of Ca II K line as an indication of the position occupied by the ribbon. Fig. 8-b clearly exemplifies the case of A1, where a substantial downflow is visible even before the ribbon itself becomes visible in the center of CaII K.

We acquired spectra with the slit in position S2 (see Fig. 2-b) from 15:46:10 until 15:48 UT. In these spectra the various bright features are all connected, and is not easy to distinguish their inner and outer edges. However, we note that the slit is tangent to A2 along its outer edge, before its second peak emission. The two spectra obtained between 15:46:10 and 15:46:20 UT along the outer edge of A2, show the Ca II K and the H_δ lines in emission with an unshifted component and a weaker and wider red shifted component. The derived velocity of this shifted, weak component is $\geq$ 50 km s^{-1}. The next spectrum,approximately

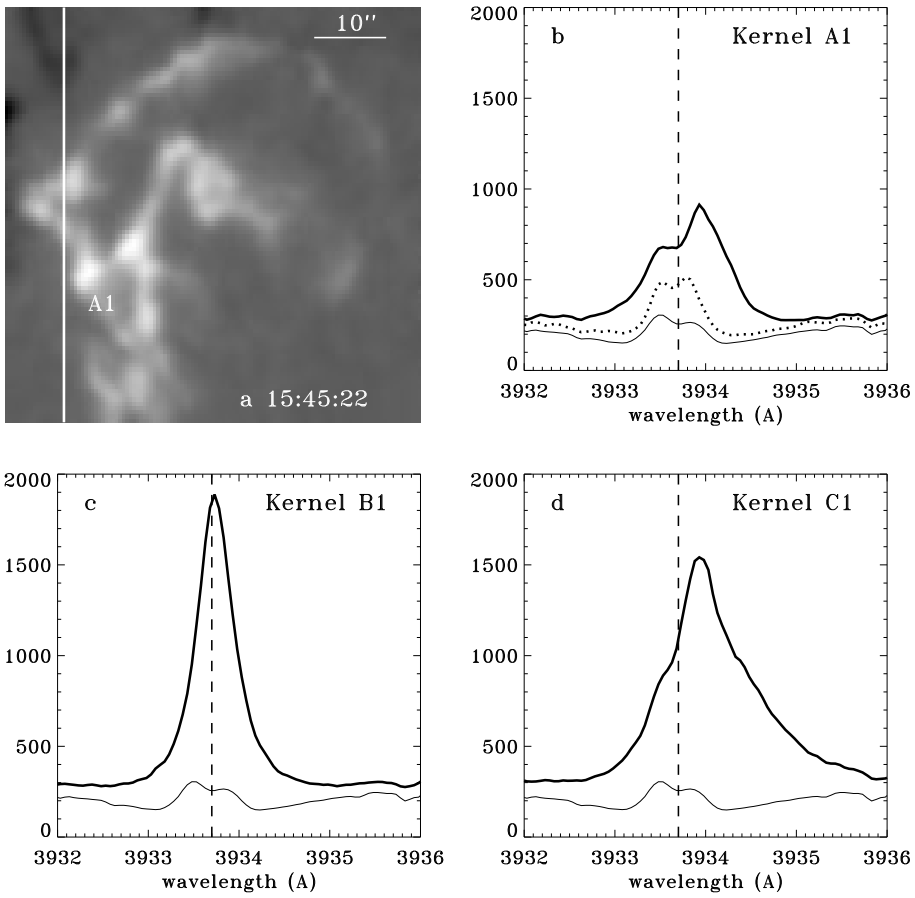

Fig. 7a–d. As Fig. 6, around the time of simultaneous maximum between A1 and A2. Now the slit touches also A1 in its outer edge. **a** H_α + 1.5 Å image; **b**, **c**, **d** CaII K profiles in a quiet region (thin line), and in kernels A1, B1, C1 (thick line). In panel **b** the A1 pre-flaring profile (dotted) is also shown

on the same position, was obtained more than one minute later (15:47:27): here both the Ca II K and the H_δ line show a red asymmetry, which, if interpreted as Doppler shift, gives a velocity of about 15 km s^{-1}. The presence of this "edge" effect seems therefore to exist for all the considered kernels, although the temporal sequence is not so clear for A2 as it is for A1.

To check for the presence of stronger velocities in the outermost points of the ribbons during other phases of the flare, we considered also the spectra acquired during the impulsive phase. The slit intersected ribbon R1 in a portion heated by conduction from the hot corona (see Fig. 4 of Paper I, and the discussion in it). Six spectra were acquired in a 30 s interval (15:43:00 to 15:43:30). For all of them the stronger downflows (20-40 km s^{-1}) are found in the outer points of the ribbon, while the inner edge shows very small or zero velocity. Fig. 8-c shows this trend at 15:43:12 UT.

5.2. Separation motion

Also during the decaying phase, the two (new) ribbons move apart from each other, away from the magnetic neutral line (see Paper I for motion during the impulsive phase). We followed the displacements of the different bright kernels in time, and traced them in Fig. 3-a with solid short lines. The arrows indicate the direction of the motion.

At the time of their maximum, both A1 and A2 move at a high separation horizontal speed ($\geq$ 40 km s^{-1} at 15:45:30 UT). Kernels B1 and C1, that slowed down immediately after the impulsive phase, now show an average velocity of about 30 km s^{-1}. A2 is the only kernel that continues to move away from the neutral line also in the final phase of the flare (after 15:49:00). Some of these horizontal velocities are shown in Fig. 9.

The kernels displacement velocities reported above are consistent with values found in the literature for two-ribbon flares. These vary from the particular case of no velocity at all (Kurokawa et al., 1992; de La Beaujardière et al., 1995), to values of about 40 km/s (Kitahara and Kurokawa, 1990). It must be said that often the reported values refer to an average over the whole ribbon, while individual kernels presumably can display faster horizontal motions, as it appears to be the case described in this paper.

5.3. What are these flows?

In Fig. 9 we summarize the ribbons dynamics, relying on kernels A1, B1 and C1 for which we have clear evidence. These kernels are all moving away from the magnetic neutral line during our observations; their separation horizontal velocities are shown in Fig. 9. On the outer edges of the flare ribbons (kernels A1 and C1, Fig. 9) we observe downflows of the order of tens

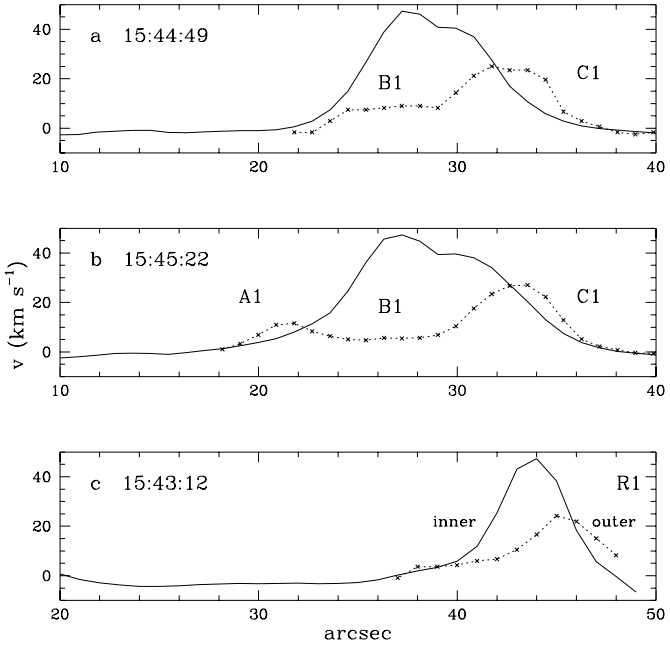

Fig. 8a–c. CaII K central intensity along the slit (solid line), and chromospheric velocity in the corresponding points (crosses). The letters indicate the position of the kernels. **a** 15:44:49, the time of Fig. 6; **b** 15:45:22, the time of Fig. 7; **c** 15:43:12, at the end of the impulsive phase

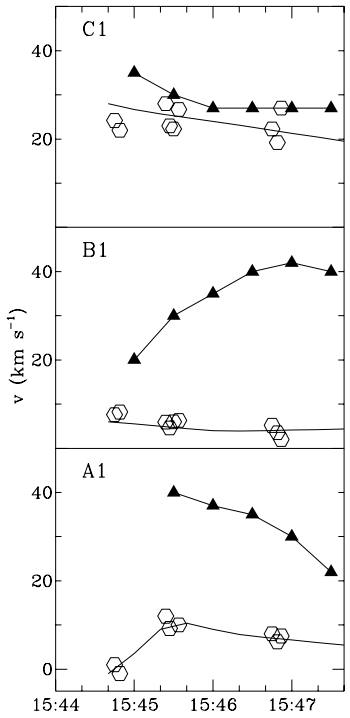

Fig. 9. Line-of-sight velocities (open symbols) in the outer edge of flaring kernels A1 and C1 and in the inner edge of B1; positive values represent downflows. Velocities away from the magnetic neutral line (filled triangles) of the same flaring kernels are also shown

of km s^{-1}, over a narrow region of 2-3″ size. These downflows seem to decrease in amplitude when the flaring kernel is slowing down (and eventually stopping) on the solar surface, as exemplified by the case of kernel A1 (Fig. 9). On the inner edge of a moving ribbon, on the contrary, we observe only very weak downflows, regardless of the horizontal velocities of the ribbon itself (kernel B1, Fig. 9). This behaviour is strongly supported by the observations in R1 during the impulsive phase (Fig. 8-c), although the short interval for which we have spectral data does not allow us to study its temporal evolution.

These signatures are consistent with the picture of two-ribbon flares, where successive magnetic reconnection episodes provide sufficient energy to heat and compress the chromosperic plasma in the outer edge of the ribbons. For the case described in this paper, the mechanism of energy transport from the coronal to the chromospheric layers is most probably conduction. In fact the presence of a hot plasma ($T_e \sim 20$ MK) in the upper part of a loop, that thermally emits in the 14-23 keV energy bands (Sect. 4.), supports the idea that the kernel A2 and B1 are heated by conduction, and suggests that conduction is the main energy transport mechanism also for other kernels like A1 and C1. We know that also the points of R1 for which we measured strong downflows (Fig. 8-c) were heated by conduction.

Reconnection models that explicity deal with the heat conduction effect (see e.g. Forbes et al., 1989; Forbes & Acton, 1996; Yokoyama & Shibata, 1997) show that the conduction front directly maps the boundary magnetic field lines. This leads to observations of hot cusp-like structures in soft X-ray (Magara et al., 1996), and of systematically higher temperatures in the outer loops of a flaring system (Tsuneta, 1996). We believe that the chromospheric downflows that we observed in the narrow regions at the outer edge of the flare ribbons map this conduction front as well. Gan et al. (1991) showed that indeed the effect of a conduction front on the chromosphere is the ablation and a simultaneous compression of the plasma, with downflows up to 100 km s^{-1}, a value consistent with our observations.

Forbes (1996, private communication), on the base of theoretical considerations, indicated a thickness of few arcsec for the locus of the downflows mapping to the conduction front. This value is consistent with our observations, that show a width of the chromospheric condensation at the edge of the ribbons of 2-3″.

6. Summary and conclusions

We have studied an eruptive, two-ribbon flare, developed around 15:43 UT on Feb. 4, 1995 in a region near disk center. We concentrate mainly on the "decay-phase", i.e. on the flare evolution after the maximum emission both in H_α and soft X-rays. We analyse coronal and chromospheric signatures, obtained with the cluster of instruments onboard *Yohkoh* and at the VTT of NSO/SP. In this later phase of the flare, we witness new episodes of coronal energy release, as proved by observations of coronal and chromospheric heating. We find convincing evidence that such energy releases are due to magnetic reconnection.

At chromospheric level we observe the development of two new flaring ribbons, in different position with respect to the ones developed in the impulsive phase. The ribbons separate from each other at an average velocity of few tens of km s^{-1}. This kind of motion, often observed, is considered one of the signatures of magnetic reconnection in the solar atmosphere.

At coronal levels we see SXR emission overlaying the whole flaring region. The analysis of the Lo-HXT and Fe XXV light curves points to a thermal origin of the HXR emission, from a source of T_e=22 MK, EM=$5.\times10^{48}$ cm^{-3}. This source is visible in the only HXT image that we could recover, as a point-like source positioned between the two new ribbons.

Within the new ribbons, several small kernels (4-6″ in size) brighten at different times; analyzing their spatially resolved H_α + 1.5 Å light curves we find a close temporal correspondence (within 2.5 s) between two pairs of kernels. We interpret this temporal coincidence assuming that each kernel pair represents the chromospheric footpoints of a coronal loop (or small system of loops) interested by the energy release, as in the case studied by Kurokawa et al. (1988). In both footpoints of the second pair of flaring kernels (maximum at 15:47:30 UT) we see He D3 emission, but no enhancement of the continuum, a signature often used to infer the site of non-thermal electrons precipitation (Cauzzi et al., 1995; Qiu et al., 1997). This fact, and the presence of a hot thermal source somewhere near the loop top at the same time, suggest that the chromospheric footpoints are heated by a conduction front. Other evidence lead us to believe that conduction from a coronal source is the mechanism responsible also for the brightening of the other kernels observed in this later phase of the flare.

The presence of a conduction front, directly related to magnetic reconnection episodes, is also consistent with an interesting, observational result of this study: from CaII K and H_δ spectra acquired in several positions across the flare, we find that the most intense chromospheric downflows are present at the *outer edge* of the ribbons. These flows have an amplitude of tens of km s^{-1}, and are observed whenever the slit crosses the outer edge of a flaring kernel or ribbon, including those observed in the flare impulsive phase. Other flaring structures show only a moderate redshift of the spectral lines, corresponding to flows of few km s^{-1}. The downward flows seem to diminish, whenever the kernels (or ribbons) slow their horizontal motion on the solar surface and fade away.

We believe that these observations provide a clear evidence of magnetic reconnection. As suggested in the classical two-ribbon flare model, and explicitily shown in recent models that consider heat conduction from the reconnecting site, the conduction front directly maps the *outer boundary* magnetic field lines of the reconnecting loops. Its effect on the chromospheric layers would be to compress the plasma, triggering downflows only on the *outer edge* of the ribbons, consistently with our observations. We are monitoring the chromospheric counterpart of the same physical effect that causes coronal (soft X-ray) cusp-like structures, and hotter coronal loops at the outer boundary of a flaring system, usually assumed as direct evidence of magnetic reconnection (see e.g. Tsuneta, 1996). Finally, our observations could provide quantitative constraints to models of coronal magnetic reconnection that take into consideration the effects of chromospheric ablation and compression from a conduction front.

Acknowledgements. We wish to thank the NSO/Sac Peak staff for the time allocation and help during the observations. NSO/Kitt Peak data used here are produced cooperatively by NSF/NOAO, NASA/GSFC and NOAA/SEL. Help with the *Yohkoh* data reduction and analysis, mainly from H. Hudson, S. Masuda, M. Morimoto (ISAS), R.D. Bentley and L.K. Harra Murnion (MSSL) is gratefully acknowledged. We thank Dr. L.A. Smaldone who contributed to the acquisition and reduction of the data. Drs. T. Forbes and R. Falciani provided very useful and lively discussions.

References

Antonucci, E. and 8 co-authors, 1982, Solar Phys. 78, 107
Aschwanden, M.J., Kosugi, T., Hudson, H.S., Wills, M.J., Schwartz, R.A., 1996, ApJ 470, 1198
Brown, J.C., 1971 Solar Phys. 18, 489
Canfield, R.C., Zarro, D.M., Metcalf, T.R., Lemen, J.R., 1990, ApJ 348, 333
Cauzzi, G., Falchi, A., Falciani, R., Smaldone, L.A., Schwartz, R.A., Hagyard, M., 1995, A&A 299, 611
Cauzzi, G., Falchi, A., Falciani, R., Smaldone, L.A., 1996, A&A 306, 625
Culhane, J.L. et al., 1991, Sol. Phys. 136, 89
de La Beaujardière, J.F., Canfield, R.C., Hudson, H.S., Wülser, J.P., 1995, ApJ 440, 386
Emslie, A.G., 1978, ApJ 224, 241
Emslie, A.G., 1983, ApJ 271, 367
Falchi A., Falciani R., Smaldone L.A., 1992, A&A 256, 255
Feldman, U., Seely, J.F., Doschek, G.A., Strong, K.T., Acton, L.W., Uchida, Y., Tsuneta, S., 1994, ApJ 424, 444
Fisher, G.H., 1989, ApJ 346, 1019
Forbes, T.G., Malherbe, J.M., Priest, E.R., 1989, Solar Phys. 120, 258
Forbes, T.G., Acton, L.W., 1996, ApJ 459, 330
Fludra, A., Doyle, J.G., Metcalf, T., Lemen, J.R., Phillips, K.J.H., Culhane, J.L., Kosugi, T., 1995, A&A 303, 914
Gan, W.Q., Fang, C., Zhang, H.Q., 1991, A&A 241, 618
Gu, X., Lin, J., Luan, T., Schmieder, B., 1992, A&A 259, 649
Hudson, H.S., 1972, Solar Phys. 24, 414
Ichimoto K., Kurokawa K., 1984, Solar Phys. 93, 105
Kitahara, T., Kurokawa, H., 1990, Solar Phys. 125, 321
Kopp, R.A., Pneumann, G., 1976, Solar Phys. 50, 85
Kosugi, T., et al., 1991, Solar Phys. 136, 17
Kosugi, T., 1993, The Yohkoh HXT Databook (I), Nat. Astr. Obs., Mitaka, Tokyo
Kurokawa, H., Takakura, T., Ohki, K., 1988, PASJ 40, 357
Kurokawa, H, and 9 co-authors, 1992, PASJ 44, L133
Magara, T., Mineshige, S., Yokoyama, T., Shibata, K., 1996, ApJ 466, 1054
Masuda, S., Kosugi, T., Hara, H., Tsuneta, S., Ogawara, Y., 1994, Nature, 371, 495
Masuda, S., 1994, Ph.D. Thesis, National Astronomical Observatory, Univ. of Tokyo
Mewe, R., Lemen, J.R., van den Oord, G.H.J., 1986, AAS, 65, 511
Moore, R. and 15 co-authors, 1980, in P.A. Sturrock (ed.), *Solar Flares*, Colorado Associated University Press, Boulder, p. 341.

Qiu, J, Falchi A., Falciani R., Cauzzi G., Smaldone L.A., 1997, Solar Phys. 172, 171 (Paper I)
Sakao, T., et al. 1992, PASJ 44, L83
Sakao, T., 1994, Ph.D. Thesis, National Astronomical Observatory, Univ. of Tokyo
Schmieder, B., Forbes, T.G., Malherbe, J.M., Machado, M.E., 1987, ApJ 317, 956
Švestka, Z., Martin, S.F., Kopp, R.A. 1980, in IAU Symp. 91, Solar and Interplanetary Dynamycs, eds. M. Dryer E. Tandberg Hanssen (Dordrecht:Reidel), 217
Švestka, Z., 1989, Solar Phys. 121, 399
Tsuneta, S., et al., 1991, Solar Phys. 136, 37
Tsuneta, S., Hara, H., Shimizu, T., Acton, L., Strong, K., Hudson, H., Ogawara, Y., 1992, PASJ 44, L63
Tsuneta, S., 1996, ApJ 456, 840
Wülser J.P., 1996, private communication
Yokoyama, T., Shibata, K., 1997, ApJ 474, L61
Yoshimori, M. et al., 1991, Solar Phys. 136, 69
Zirin, H., 1988 in: Astrophysics of the Sun, Cambridge University Press, Cambridge

This article was processed by the author using Springer-Verlag LaTeX A&A style file *L-AA* version 3.